AEROELASTIC SIMULATION OF S-DUCT DYNAMICS USING STRUCTURE-COUPLED CFD

Jonathan Smith , Mats Dalenbring
***FOI, Swedish Defence Research Agency, SE-164 90 Stockholm**

Keywords: *Fluid-Structure-Interaction, Aeroelastic, CFD, UAV, S-duct*

Abstract

Results are presented for a computational study of dynamic aeroelastic effects in the S-duct outlet nozzle of a low-observable unmanned air vehicle (UAV). Elastodynamic models, including the use of layered, radar absorbing structures (RAS), are analysed and used to generate a modal basis. The modal structural model is then used, coupled to an unstructured CFD flow solver, in a time-domain aeroelastic simulation. Results are presented for both stable response and limit cycle oscillations (LCO). By varying the properties of the structural model it is demonstrated that this technique can be used as a design tool, for predicting the dynamic response of similar duct-like structures containing high-speed, unsteady flows.

1 Introduction

Computational aeroelastic simulation, using fluid-structure coupled CFD, is an established technique for aircraft aeroelasticity, in particular for the analysis of nonlinear, transonic flutter. We present a new application of this technology in the design of propulsion systems in low-observable, unmanned air vehicles (UAV) in which the engine face and exhaust are hidden from radar and infra-red (IR) sensors by means of curved, S-duct channels. The design of S-duct channels is complicated since the internal curvature can result in regions of unsteady, separated flow which endanger engine performance. However, almost all CFD-studies to date have been restricted to steady-state flow solutions for rigid geometries. We argue that, due to the sensitivity of S-duct flows and the use of extreme lightweight construction, it is also necessary to model dynamic aeroelastic effects. To this end, we present a series of aeroelastic simulations using structure-coupled CFD.

The work presented here is part of a larger project [14] studying Propulsion Integration for low-observable UAV systems. This project is part of the research programme *FoT-25* funded by FMV[1] and is coordinated by the Volvo Aero Corporation. The project is based on the design of a low-observable UAV configuration co-denamed *Eikon*. Published work on this configuration includes both computational and experimental Aerodynamics [21] and analysis of radar and Infra Red signatures [15, 14]. The present study concerns the *Eikon* outlet nozzle and S-duct but follows a similar aeroelastic analysis of the air intake channel [5].

The arrangement of the S-duct channels in *Eikon* is shown schematically in figure 1. The inlet and outlet channels meet the cylindrical engine region in circular interface planes of radius 0.35 m. The outlet channel and nozzle unit is 2.3 m long and has a roughly elliptical exit aperture, which is shrouded by V-shaped, tapered upper and lower surfaces.

The results presented here are based on two preliminary structural models used early in the development of the *Eikon* propulsion concept. It must be emphasised that neither of these models is representative of the current *Eikon* design, the

[1] FMV: The Swedish Defence Materiel Administration

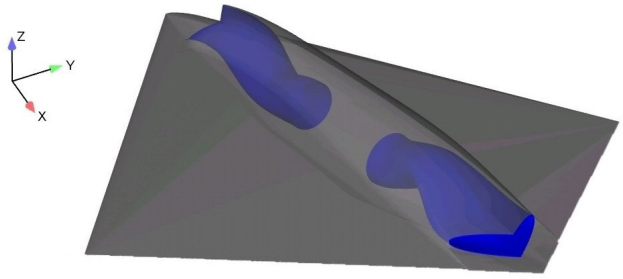

Fig. 1 Internal surfaces of inlet and outlet channels in the *Eikon* configuration (schematic).

details of which are confidential. However, the properties of these models are sufficiently realistic to demonstrate the computational method and its applicability in the design process.

2 Computational Resources

The computational tools used here are CFD flow-solver Edge [7] and the structural Finite Element (FE) structural analysis code Stripe [1], both of which are developed and maintained by FOI. The structural analysis program Stripe features *hp*-adaption and advanced functions for large-scale computations for fracture and damage analysis. The development of the Stripe code and it's underlying methodology are described in [2, 6]. For a more general treatment of *hp*-adaptive methods see [16, 20, 18]. The CFD code, Edge, with its unstructured, dual mesh formulation, is capable of solving flow systems, including RANS[1] and DES[2], for complex geometries. More information about Edge is provided on the FOI website[3].

The calculations presented here are based on time-accurate, Euler flow solutions using Edge with its recently-introduced functions for modal, aeroelastic coupling. The inputs for these computations are the CFD mesh, the aerodynamic conditions and a normal-modes respresentation of the structure. The Stripe code is used both to compute the normal modes and to interpolate the structural modeshapes onto the surface points of the CFD grid. This separation of the structural and fluid computations is standard practice in aeroelastic problems and is made possible by the use of a linear elastodynamic model.

Both Edge and Stripe are fully scalable codes, which can be efficiently used for high-volume computations on parallel machines with large numbers of processors. However, in the present study, the fluid and structural models are both relatively small and computations were restricted four processors throughout. For the dynamic aeroelastic simulations, performed on an AMD64 Opteron cluster, the run-time was roughly six hours per second of simulated time.

3 Structural and Aeroelastic Model

3.1 CFD Model and Structural Coupling

The Aeroelastic functionality in Edge used in the present study is fully described in the FOI report [17]. A brief summary now follows.

3.1.1 Computational Method

For the coupled simulation, the structural model is represented in terms of the elastic modes of the undamped system so that the equation of motion can be written in the form

$$\ddot{q}_k + 2\zeta_k \omega_k \dot{q}_k + \omega_k^2 q_k = \frac{1}{a_k} Q_k \qquad (1)$$

where the scalar terms $q_k(t)$ and Q_k are the modal coordinates and generalised forces and ω_k, ζ_k and a_k are respectively the angular frequency, damping ratio and generalised mass for mode k. The generalised mass terms a_k arise as normalisation constants for the elastic modes of the structural model, a set of orthogonal shape functions. For an inviscid flow calculation, the modal force is computed as the surface integral

$$Q_k(t) = \oint_{S(t)} (\delta \mathbf{x}_k) \cdot p(t) \mathrm{d}\mathbf{S} \qquad (2)$$

where $p(t)$ is the local value of the fluid pressure and $\delta \mathbf{x}_k$ is the constant, surface displacement for the modeshape of mode k.

[1] Reynolds Averaged Navier Stokes
[2] Detached Eddy Simulation
[3] www.foi.se/edge See also FOI publications.

The time-domain coupling of the reduced, modal structural model and the CFD flow solver is achieved using a conventional staggered scheme (CSS) [8] exploiting the dual time-stepping algorithm used for time-integration of the flow equations [11]. At each physical timestep, the fluid and structural equations of motion are converged in an inner-loop iterative process. This allows the coupled fluid and structural domains to be accurately synchronised and the physical timestep to be chosen based on the dynamical properties of the structural model.

To provide the spatial coupling of the between the fluid and structural solvers it is necessary to provide a physically consistent interpolation scheme for exchanging the fluid loads and structural surface displacements at the moving boundary surface. This is problem, which arises because the two solvers operate on independent grids, is in general quite complex. However, for the models used in this study, the separation between the surface points in the structural and fluid grids is very small. It was therefore chosen to use an interpolation scheme directly exploiting the polynomial basis functions of the Stripe FE-code, with a direct element-neighbour search to establish the inter-grid connectivity.

To maintain continuity with the moving, elastic boundary surface, it is necessary to dynamically adjust the entire CFD mesh. In Edge this can be done by first computing a set of constant "perturbation fields", one for each elastic mode. During the simulaton the mesh coordinates field $X(t)$ is computed directly from the modal coordinates in the form

$$X(t) = X_0 + \sum_{k=1}^{N} (\Delta X)_k \, q_k(t) \qquad (3)$$

where X_0 is the coordinates field of the base mesh and $(\Delta X)_k$ is the perturbation field for mode k. This method places the, computationally expensive, mesh deformation process off-line. However, the flow solution is obtained using a dual mesh, each cell of which encloses a node of the primary mesh. During the coupled simulation process, the surfaces of these control volumes must therefore be recomputed each time the motion of elastic surface is updated [17].

3.1.2 CFD Mesh and Boundary Conditions

Boundary Conditions The CFD model represents the internal flow in outlet channel. A mass-flow boundary condition [13] is used at the inlet plane and a free static pressure boundary at the outlet surface. The primary mesh is assembled from tetrahedral elements and has 1.1e5 nodes. For all flow solutions, the boundary conditions are as shown in table 1, matching the main design point [21] of the *Eikon* propulsion system: maximum power flight at sea level.

Mesh Deformation To obtain the modal, mesh-perturbation fields, in equation 3, the primary volume mesh was deformed using a quasi-elastic method with an edge-based algorithm [3] which exploits the metrics of the undeflected dual mesh. Each elastic mode was scaled to the maximum displacement achievable without creating negative cells, with a matching adjustment of the modal generalised mass. For the mesh deformation, the inlet surface was fixed as a sliding plane whilst the outlet surface was unconstrained [9].

3.2 Structural Model and Normal Modes

The structure of the *Eikon* outlet is represented by two FE-models, denoted O1 and O2, from which the first ten normal modes are extracted using a modified Lanczos [10] algorithm. For the coupled simulations the resulting modal systems are modified by addition of viscous damping as defined in equation 1. The surface meshes of the two FE-models are shown in figure 2 together with the modeshapes of the first four modes, scaled to unit generalised mass. For all these

interior surface	Euler wall	
Inlet plane	mass-flow	62.5 kg/s
	temperature	700 K
Outlet surface	static pressure	free stream

Table 1 Boundary conditions for Edge CFD computations (*Eikon* maximum power design point)

modes the surface motion is predominantly in the Z and X (vertical and streamwise) directions.

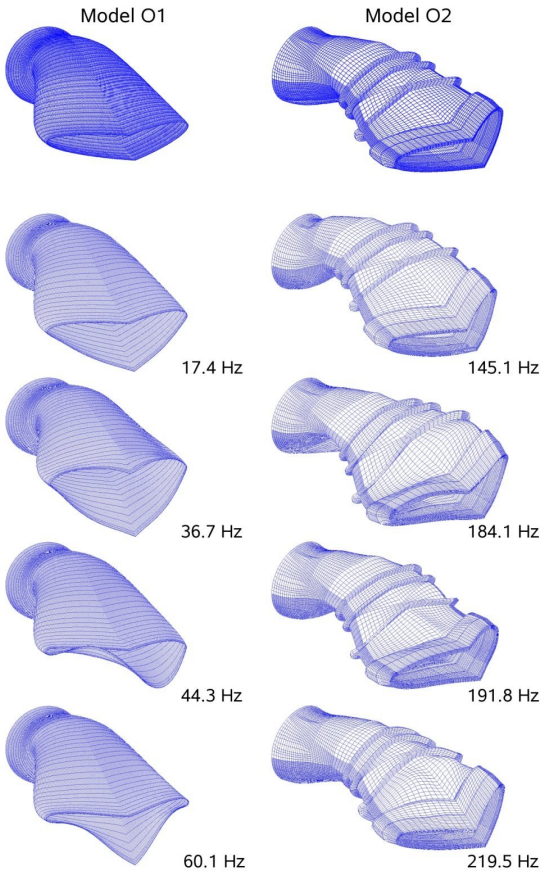

Fig. 2 Surface meshes and first four modeshapes for structural models O1 and O2

The first structural model, O1, total mass 110 kg, represents a single shell of uniform thickness of 3 mm, made of a temperature resistant superalloy of type Inconel 706 ($\rho = 8100$ kgm^{-3}, E = 210 GPa, $\nu = 0.38$). The structure is clamped at the inlet plane but is otherwise unconstrained. The second model, O2, total mass 220 kg, represents a more realistic, radar absorbing structure (RAS) [19] with a bonded sandwich structure comprising two outer plates of thickness 1 mm enclosing a distance-material layer of thickness 7 mm. The exterior of the structure is augmented with six ring stiffeners and three small axial stiffeners under the lower surface of the outlet nozzle. The greater complexity of the O2 model is reflected in the number of elements, 5500 compared to 3000 for model O1. The O2 structure is clamped at the inlet plane and an axial sliding boundary condition is set at five positions at the rear end of the structure. The finite element model of this layered structure uses a 3-D homogenised approximation with effective planar isotropic elastic properities [4].

4 Simulation Results and Analysis

4.1 Static Coupled Simulations

Static coupled simulations were carried out by setting the structural damping terms, ζ_k in equation 1, to unity, thus eliminating any oscillatory structural response. For these simulations the timestep was set to 0.01 s and adequate convergence to the equilibrium state is achieved in less that 1 s of model time. All simulations were carried out using the boundary conditions given in table 1 and initiated from a single, steady-state solution for the rigid geometry. Figure 3 shows surface pressure and Mach number distributions for steady state solutions obtained with the rigid geometry and models O1 and O2.

The rigid surface results show that the internal flow is choked, with a supersonic region extending about 0.5 m upstream of the outlet aperture. This results in very large internal pressures and structural loads. Furthermore, time-accurate solutions show that this flow is also highly unsteady, even with a completely rigid geometry. Similar results are obtained for a wide range of inlet mass flow and temperatures. The results for both static coupled solutions show clear evidence of structural interaction, including a substantial change in the surface pressure distribution.

With model O2, the excess internal pressure results in balloon-like expansion of the structure about 0.2 m upstream of the outlet. Near the outlet, however, the extra wall stiffening preserves the aperture shape. In contrast, the model O1 structure is much more flexible and the effect of the internal pressure loading is to widen the outlet channel in the vertical direction. This moves the effective nozzle aperture upstream, causing a large reduction of the internal pressure.

These static simulaton results alone provide information which is useful for design purposes.

For example, it can be seen that the O1 structure is underdiminsioned indicating that to contain the flow, it must be made stiffer, especially in the section near the nozzle exit. The O2 structure is much more robust and gross vertical displacements are eliminated by the boundary conditions of the model. However, even with this structure, additional stiffening is required, particularly in the region showing the large inflationary deformation, just upstream of the exit aperture.

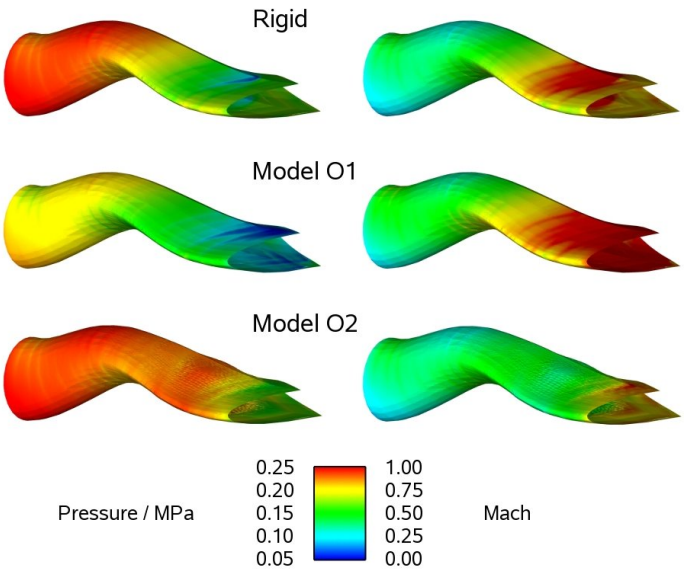

Fig. 3 Steady-state surface pressure and Mach number distributions for the rigid geometry and static equilibrium states of models O1 and O2

4.2 Dynamic Coupled Simulations

Dynamic coupled simulations were carried out, each starting from the appropriate static-coupled, steady state solution. For model O2, the structure was excited by imposing, at t = 10ms, an initial velocity of in mode 1 equivalent to a maximum displacement amplitude of 0.1 m for the undamped structure. For model O1, the coupled system was found to be highly sensitive and required no excitation other than that produced by the unsteady flow. For each structural model, five separate coupled simulations were obtained with different settings of the structural damping parameters, ζ_k in equation 1. Uniform modal damping was used throughout, with the values $\zeta = 0, 0.01, 0.02, 0.05, 0.10$. The same physical timestep was used for both models, $\Delta t = 0.2$ ms, thus resolving of the highest structural modes at at least 10 points per cycle. The inner loop was set to 40 iterations, which was shown to give adequate convergence for all simulations. Where possible, the simulations were was extended to 1.5 s. Results from these dynamic simulations are presented in figures 4 and 5 and in table 2.

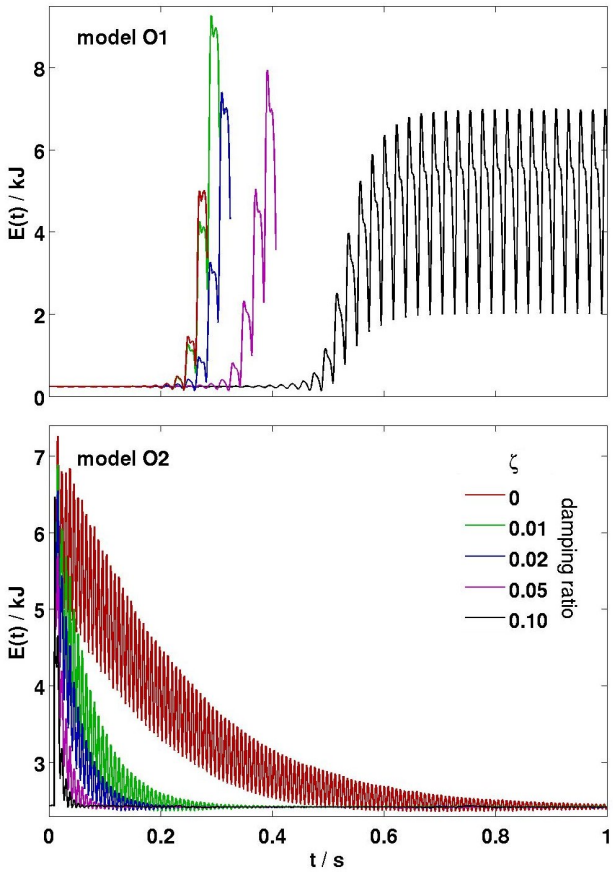

Fig. 4 Structural Energy timeseries for simulations with different levels of structural damping

Figure 4 shows timeseries of the total structural energy, for both structural models and all five damping cases. The structural energy terms are calculated from the modal parameters and coordinates timeseries [17, 9]. For model O1, the coupled system is unstable and for all but the most strongly damped case the amplitude of oscillation is so large that the solution terminated due to inverted cells in the CFD mesh. However, with 10% structural damping, the solution reaches a sustained limit cycle. For model O2,

the response is oscillatory but decays in amplitude even with zero structural damping, showing that for this system the aerodynamic forces are stabilising. This is to be expected given the choked flow in the nozzle and the well-contained form of the static coupled solution (see figure 3).

Table 2 shows values of the maximum surface displacement and maximum displacement amplitude for selected time intervals. For model O2, the sample is taken immediately after excitation. For model O1, the sample is the last 20 ms of each simulation as shown in figure4. The amplitude estimate used is the standard deviation of the displacement timeseries, at each structural node.

	model O1		model O2	
ζ	disp./m	ampl./m	disp./m	ampl./m
0.00	0.304	9.7e-02	0.160	5.1e-02
0.01	0.416	1.3e-01	0.156	4.8e-02
0.02	0.370	1.2e-01	0.152	4.6e-02
0.05	0.364	1.1e-01	0.140	3.9e-02
0.10	0.317	9.2e-02	0.125	3.0e-02

Table 2 Maximum displacement and maximum amplitude estimates for 20 ms sample intervals.

For model O1, the displacements are very large compared to the size of the model, even for the high damping cases and an oscillation of this amplitude would certainly result in rapid structural failure. For model O2, the values are more realistic and the increased structural damping gives a progressive reduction in amplitude.

Figure 5 shows, for each structural model, a frequency-domain representation of the response at 5% structural damping, together with the line spectrum of the normal modes of the free structure. The response spectra show, for each mode, the modulus of the discrete Fourier transform of the modal coordinate timeseries. The modal response is factored by the (constant) RMS value of the modeshape surface displacement.

From the spectra in figure 5 it can be seen the low frequency and static response of model O1 is dominated by its first two structural modes. For model O2, however, this region is dominated by modes 1 and 4. Both these observations are

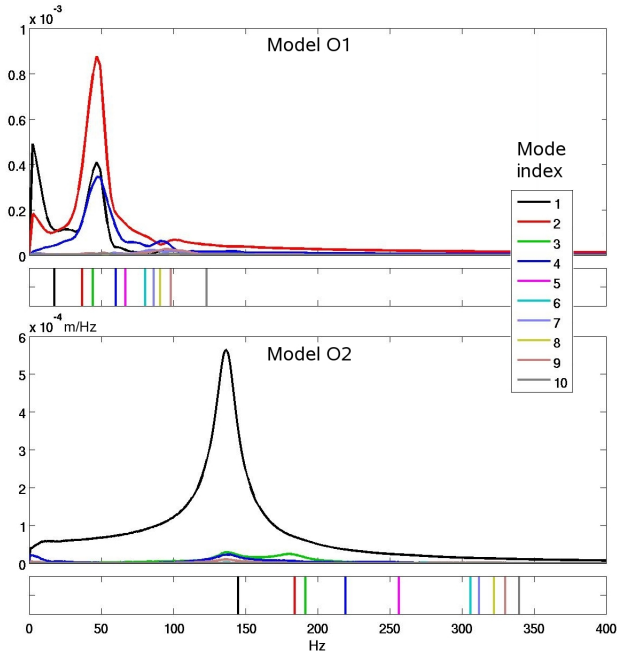

Fig. 5 Modal response spectra for coupled solutions at 2% structural damping, compared to line spectra for the undamped structural model.

consistent with the surface shapes shown in figures 2 and 3. The dynamic response of each model is dominated by a single frequency: 48 Hz for model O1 and 136 Hz for model O2. However, the characteristics of the two systems are quite different. The response of model O2 is essentially a damped, single degree of freedom system and is almost entirely in the first structural mode. For model O1, the aerodynamically excited oscillation arises through a mechanism coupling structural modes 1, 2 and 4. For the sustained LCO in the 10% damping case, there is a much sharper response peak at a slightly lower frequency, 46 Hz, with strong harmonics at 91, 136 and 182 Hz. For model O2 the response frequency is less sensitive to the structural damping, being constant to within 0.5 Hz in all cases.

For both models, the response spectra clearly show the effects of aerodynamic coupling between the structural modes. Most obviously, each of the large response peaks is echoed in the other modal spectra. Furthermore the response is dominated by a small subset of the structural modes with no visible response from modes of intermediate frequency. The frequencies of the par-

ticipating modes are also shifted from the free-structure values and the size and direction of the shift cannot be accounted for by the added structural damping. The fluid-coupled model represents a new dynamical system.

5 Conclusions and Future Work

Conclusions The results presented in section 4 demonstrate that aeroelastic simulation using structure-coupled CFD can, in principle, be applied to the design of S-duct and nozzle structures. It has been shown that coupling the CFD and structural models produces a hybrid system with dynamic behaviour which could not be predicted using separate fluid and structural models. In this instance, the effects are severe, including large deflections and unstable oscillatory cycles. However, these effects can be alleviated by changing structural parameters, such as the shell thickness and structural damping. The stability of any updated design can be re-evaluated by repeating the simulation process.

The large structural deformations produced in the simulations here demonstrate the robustness of the mesh deformation technique, at least for the present Euler mesh. It would therefore be possible, in principle, to extend the technique using a non-linear structural model specifically for large deformations.

For initial design purposes, static coupled CFD simulations provide and effective tool for dimensioning the structure. The run time for such a simulation is only slightly greater than that of a conventional rigid surface calculation with the same CFD model. For a relatively coarse, mesh as used here, it would be feasible to carry out a parametric study with a large number of structural cases. Dynamic coupled simulations could be used at a later stage in the design process to evaluate the stability of the system. Dynamic simulations require longer run times, however, if the structure has first been dimensioned for the static loads, the dynamic effects should be relatively small and fewer of these computations would be necessary.

The fluid-structure interaction techniques presented here provide a means for modelling duct and nozzle structures for containing high speed flows. The use of these techniques early in the design cycle could enable such structures to be developed at substantially reduced risk.

Future Work The most obvious extension of the techniques presented here would be to extend upgrade the CFD model to a viscous RANS flow. The effect of viscous forces is undoubtedly significant, especially so for S-duct systems vortex generator arrays [12]. Coupled simulations could be used to examine the sensitivity of these systems to structural vibration. However, using a RANS flow model requires a much greater computational resource for the flow solution and the additional difficulty of deforming a high resolution mesh with a resolved boundary layer. Such computations could only be used for detailed study of isolated cases.

For more immediate applications, substantial improvements can be made in automating the process of setting up the fluid structure coupling and analysing the dynamic response data from, more affordable, inviscid flow simulations.

References

[1] Andersson B, Falk U, Babuska I, and von Petersdorff T. Reliable Stress and Fracture Mechanics Analysis of Complex Components Using a h-p Version of FEM. *International Journal for Numerical Methods in Engineering*, Vol. 38, 1995.

[2] Andersson B, Falk U, and Jarlås R. Self-adaptive FE-analysis of solid structures, Part I: Element formulation and a posteriori error estimation. Technical report, FFA, 1986.

[3] Berggren M. Edge-based mesh movement strategies. unpublished preprint.

[4] Dalenbring M. Analysis of Materials and Structures used within the FoT25 Project Propulsion Integration. Technical report, FOI, 2006. (in manuscript).

[5] Dalenbring M and Smith J. Simulation of S-Duct Dynamics using Fluid-Strucutred Coupled CFD. *AIAA-2006-2981*, 2006.

[6] Dalenbring M and Zdunek A. On the use of three-dimensional h- and p-version finite elements in solving vibration response problems. *Journal of Sound and Vibration*, Vol. 288, 2005.

[7] Eliasson P. EDGE, a Navier-Stokes solver for unstructured grids. *Proc Proc. of Finite Volumes for Complex Applications III*, pp 527–534, 2002. ISBN 1 9039 9634 1.

[8] Farhat C, Lesoinne M, and Maman N. Mixed explicit/implicit time integration of coupled aeroelastic problems: three-field formulation, geometric conservation and distributed solution. *Internat. J. Numer. Methods Fluids*, Vol. 21, No 10, pp 807–835, 1995.

[9] FOI. *Edge 4.0 Manual, Issue 4.4.0, dnr. 03-2870*, May 2006.

[10] Hughes J. *The Finite Element Method*. Prentice-Hall, Inc., 1987. ISBN 0-13-317025-X.

[11] Jameson A. Time Dependent Calculations Using Multigrid with Applications to Unsteady Flows Past Airfoils and Wings. *AIAA Paper*, , No 91, pp 1596, June 1991.

[12] Jirásek A. A modified vortex generator model and its application to complex aerodynamic flows. Technical Report FOI-R-1204-SE, FOI, 2004.

[13] Jirásek A. Mass Flow Boundary Conditions for Subsonic Inflow and Outflow Boundary. AIAA Paper 2005-4963, 23rd AIAA Applied Aerodynamics Conference and Exhibit, Toronto, Ontario, Canada, 2005.

[14] Johansson M. Propulsion Integration in an UAV. *AIAA-2006-2834*, 2006.

[15] Johansson M and Dalenbring M. SIGGE, a prediction tool for aeronautical IR signatures, and its applications. *AIAA-2006-3276*, 2006.

[16] Oden J. T, Demkowicz L, Rachowicz W, and Westermann T. A. Towards a universal hp-adaptive finite element strategy, Part 2: A posteriori error estimation. *Computational Methods in Applied Engineering*, 1989.

[17] Smith J. Aeroelastic fucntionality in Edge, Initial implementation and validation. Technical Report FOI-R-1485-SE, FOI, December 2005.

[18] Solin P, Segeth K, and Dolezel I. *Higher-Order Finitie Element methods*. Chapman and Hall / CRC Press, 2003.

[19] Stonier R. A. Stealth Aircraft and Technology from World War II to the Gulf, Part II: Applications and Design. *SAMPE Journal*, Vol. 27, 1991.

[20] Szabo B and Babuska I. *Finite Element Analysis*. John Wiley and Sons Inc. New York, 1991. ISBN 0-471-50273-1.

[21] Tormalm M. Design and Ananlysis of Compact UAV Ducts. *AIAA-2006-2828*, 2006.